Crystallography of Martensite in Friction-Stir-Welded 12Cr Heat-Resistant Steel

PENG HUA, SERGEY MIRONOV, YUTAKA S. SATO, HIROYUKI KOKAWA, SEUNG HWANG C. PARK, and SATOSHI HIRANO

In this work, electron backscatter diffraction (EBSD) was applied for examination of the crystallography of the martensitic structure produced during friction-stir welding (FSW) of 12Cr heat-resistant steel. The martensitic transformation was found to be governed by the Kurdjumov–Sachs (K-S) relation, *viz.* $\{111\}\gamma \parallel \{110\}_{\alpha'}$ and $\langle 110\rangle\gamma \parallel \langle 111\rangle_{\alpha'}$, was characterized by substantial variant selection and led to considerable orientation spread within the martensite variants. Due to the latter effect, the K-S model was found to be ineffective for the reconstruction of prior-austenite grain structure. Instead, the mixed orientation relation, *viz.* $\{111\}\gamma \parallel \{110\}_{\alpha'}$, $\langle 110\rangle\gamma \parallel \langle 111\rangle_{\alpha'}$, and $\langle 112\rangle\gamma \parallel \langle 110\rangle_{\alpha'}$, was shown to be more suitable for this purpose.

https://doi.org/10.1007/s11661-019-05220-1

I. INTRODUCTION

THE 12Cr steel belongs to a recent generation of heat-resistant ferritic steel. Due to an excellent combination of high creep-rupture strength and good corrosion and oxidation resistance, it is often considered as a very promising structural material for the power industry.[1–5] Unfortunately, the unique properties of this material are totally degraded during conventional fusion welding due to hydrogen-induced cracking, porosity, formation of delta-ferrite, as well as dissolution of strengthening precipitates associated with the solidification process.[6–12] Friction-stir welding (FSW), being an innovative solid-state joining technique, enables avoiding (or minimizing, at least) these problems and thus principally improving the welding quality. The first works in this area have demonstrated excellent feasibility of this technique for joining of 12Cr steel,[13–20] thus necessitating a more fundamental understanding of the underlying physical processes. Specifically, it has been found that the peak FSW temperature normally exceeds the A_3 point; therefore, the final weld microstructure is produced by the martensitic transformation occurring during the weld cooling cycle (*e.g.*, Reference 14). For such transformations, the properties of the resulting material are known to be essentially influenced by a crystallographic relationship between the high-temperature and low-temperature phases. In friction-stir-welded 12Cr steel, however, crystallography of the martensitic structure has not been examined so far, to the best of the authors' knowledge. It has been suggested that the unique character of the FSW process, which involves very large strains at high temperature, and high strain rate may exert an essential influence on the martensitic transformation. Attempting to improve the basic physical understanding of the microstructural processes in this case, the present work focused on this issue.

II. EXPERIMENTAL

The program material used in the present study (Fe-0.14C-12Cr-0.2V-0.1Nb-0.05N, all in wt pct) was supplied as 3-mm-thick sheets. In the received condition, the material had tempered martensitic structure with $M_{23}C_6$ carbides precipitated along grain boundaries and the nanoscale MX dispersoids evenly distributed in the grain interior. The original microstructure has been described in

PENG HUA is with the School of Materials Science and Engineering, Hefei University of Technology, 193 Tunxi Road, Hefei 230009, P.R. China, and also with the Department of Materials Processing, Graduate School of Engineering, Tohoku University, 6-6-02 Aramaki-aza-Aoba, Aoba-ku, Sendai 980-8579, Japan. Contact email: weldinghua@163.com SERGEY MIRONOV is with the Department of Materials Processing, Graduate School of Engineering, Tohoku University, and also with the Belgorod National Research University, Pobeda 85, Belgorod 308015, Russia. YUTAKA S. SATO is with the Department of Materials Processing, Graduate School of Engineering, Tohoku University. HIROYUKI KOKAWA is with the Department of Materials Processing, Graduate School of Engineering, Tohoku University, and also with the School of Materials Science and Engineering, Shanghai Jiao Tong University, 800 Dongchuan Road, Minhang District, Shanghai 200240, P.R. China. SEUNG HWANG C. PARK and SATOSHI HIRANO are with the Hitachi Research Laboratory, Hitachi Ltd, Omika 7-1-1, Hitachi 319-1292, Japan.

Manuscript submitted November 29, 2018.
Article published online April 22, 2019

more detail elsewhere.[14] The supplied material was friction-stir welded in bead-on-plate configuration at the tool rotational rate of 400 rev min^{-1} and the tool travel speed of 200 mm min^{-1}. The welding tool was fabricated from a polycrystalline cubic boron nitride and consisted of a scrolled shoulder of 24 mm in diameter and a step spiral (SC4) probe of 2.8 mm in length. To prevent surface oxidation, the welding process was performed in an argon atmosphere. For microstructural observations, the produced welds were sectioned perpendicular to the welding direction (WD), mechanically polished in a conventional fashion with a final step involving 24-hour vibratory polishing with colloidal silica suspension. Microstructural examinations were focused in the central section of the stir zone and were conducted by using the electron backscatter diffraction (EBSD) technique. To this end, a JSM-7800F field-emission-gun scanning electron microscope equipped with a TSL OIM* EBSD system was used at an accelerating voltage of 25 kV and a scan step size of 0.1 μm. The α'-martensite was indexed as a body-centered-cubic phase; this approach is believed to be feasible for the EBSD of steels.[21 25]

*TSL OIM is a trademark of TexSEM Labs Orientation Imaging Microscopy.

III. RESULTS AND DISCUSSION

A. *Orientation Relationship*

An EBSD orientation map taken from the central section of the stir zone is shown in Figure 1(a). In the map, martensite crystals are colored according to their crystallographic orientations relative to the WD (the color code triangle is given the upper right corner) and low- and high-angle boundaries (below and above 15 deg, respectively) are depicted as white and black lines, respectively. (Here and hereafter, the reader is referred to the on-line version of the paper to see the figures in color). As shown in the previous work,[14] this microstructure was nearly fully martensitic. Indeed, a complex hierarchical structure consisting of prior-austenite grains, martensite packets, and martensite blocks may be recognized in Figure 1(a).

On the other hand, EBSD mapping also revealed a minor fraction (~ 0.1 pct) of austenite retained at the martensite grain boundaries (Figure 1(b)). This enabled examination of a local orientation relationship between the austenite and the martensite. Typically, this is described in terms of either the Kurdjumov–Sachs (K-S) relation, *viz.* $\{111\}\gamma \parallel \{110\}_{\alpha'}$ and $\langle 110\rangle\gamma \parallel \langle 111\rangle_{\alpha'}$, or the Nishiyama–Wasserman (N-W) relation, *viz.* $\{111\}\gamma \parallel \{110\}_{\alpha'}$ and $\langle 112\rangle\gamma \parallel \langle 110\rangle_{\alpha'}$. To examine these possibilities, appropriate pole figures were compared, as exemplified in Figure 1(c); for clarity, crystallographic directions in the austenite that are close to that of the α'-martensite are circled. It is seen that the measured orientations of the α'-martensite satisfied neither the ideal K-S nor the N-W model but rather lay between these two.

To gain additional insight into this issue, the martensite orientation data were extracted from several prior-austenite grains and compared with ideal orientations of the martensite variants expected from the K-S and N-W orientation relationships. A typical example is shown in Figure 2. Specifically, Figures 2(a) and (b)

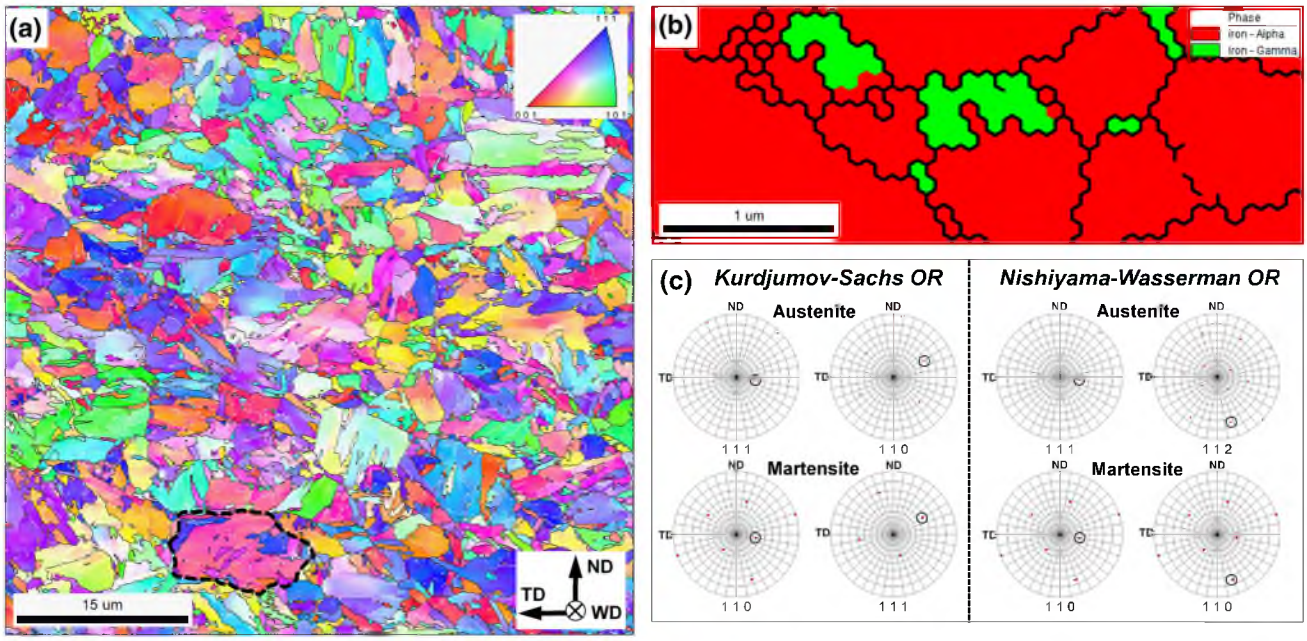

Fig. 1—Microstructural characterization of the stir zone: (*a*) EBSD orientation map (color code triangle is given in the top right corner) taken from the central section of the stir zone, (*b*) selected portion of the EBSD phase map illustrating retained austenite, and (*c*) pole figures showing the local orientation relationship between the retained austenite and the martensite. In (a), selected area exemplifies a prior-austenite grain. In (c), the closest related directions in the austenite and the martensite are circled. WD, TD, and ND are welding direction, transverse direction, and normal direction, respectively (Color figure online).

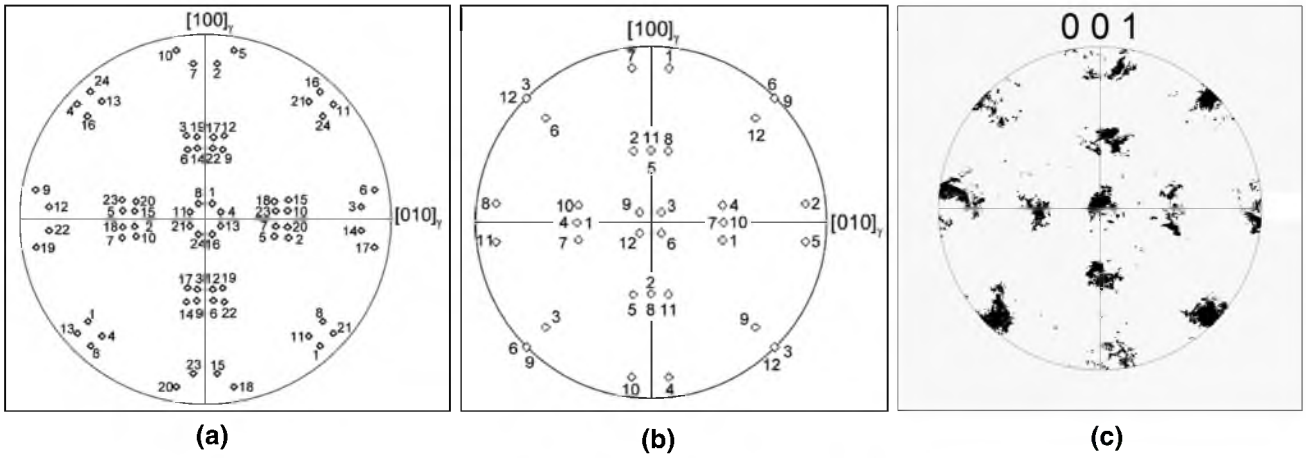

Fig. 2—Ideal 100 pole figures expected for the (*a*) K-S orientation relationship and (*b*) N-W orientation relationship,[15,16] and (*c*) the measured 100 pole figure derived from a single prior-austenite grain. The numbers in (a) and (b) indicate martensite variants. Note: The measured pole figure was appropriately rotated to facilitate comparison with the ideal pole figures.

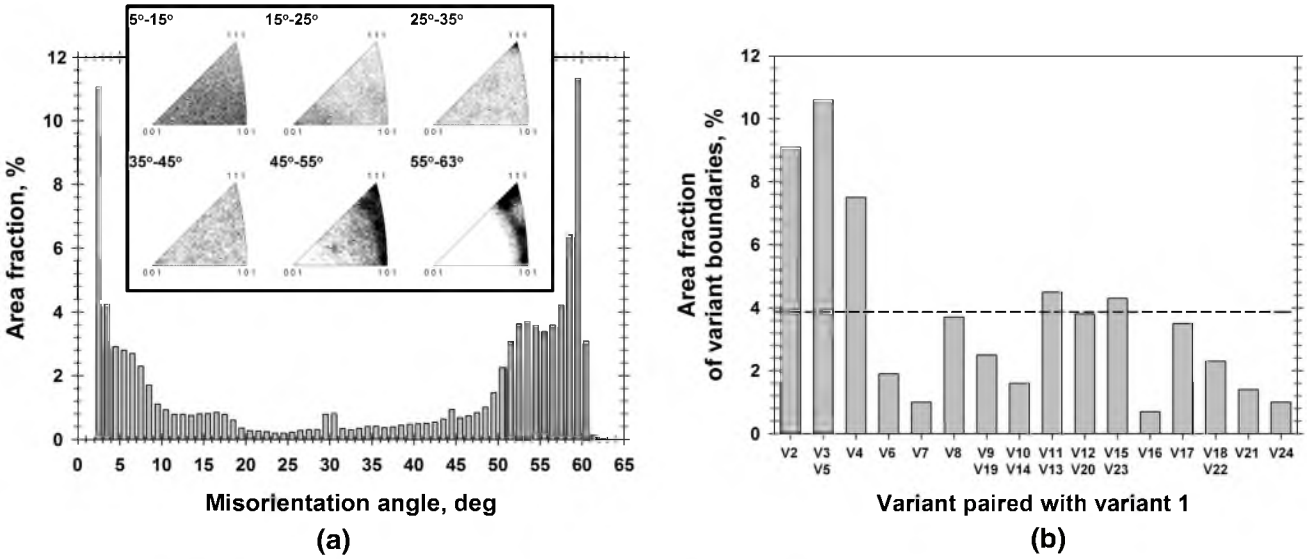

Fig. 3—(*a*) Misorientation distribution and (*b*) variant-pairing-frequency histogram derived from the martensitic phase. In the upper section of (a), the misorientation-axis distribution is shown as an inset. In (b), the horizontal broken line represents the fraction of the intervariant misorientations expected for a random distribution of variants (*i.e.*, no-variant-selection condition).

illustrate the ideal orientations of the martensitic variants (indicated by numbers) inherent from a single parent austenite grain according to the K-S and N-W relationships, respectively, whereas Figure 2(c) shows experimental data. It is clear that the measured martensite orientations were characterized by significant orientation spread, which resulted in essential overlapping of the orientations expected from the K-S and N-W relationships and thus confounded the unambiguous interpretation of the orientation relation. This observation is thought to be attributable to the significant dilatation effect inherent to the martensitic transformations and the concomitant strains induced within the martensite crystals. Nevertheless, considering a characteristic circular appearance of the measured martensite orientations (Figure 2(c)), the orientation relationship was suggested to be closer to the K-S (Figure 2(a)) rather than to the N-W (Figure 2(b)).

B. *Misorientation Distribution*

Attempting to explore the mechanism of the martensitic transformation in further detail, martensite misorientation data were derived from the EBSD map and are summarized in Figure 3(a).

The revealed misorientation distribution was very specific with a sharp low-angle peak and pronounced maxima at 50 to 60 deg as well as clustering of rotational axes near the ⟨111⟩ and ⟨110⟩ poles. Assuming that the α'-martensite was produced during the weld cooling cycle and thus experienced no significant strain during FSW, the unusual character of the measured

distribution can be attributed to misorientations between martensite variants. Due to the crystal symmetry of the γ and α' phases, there are 24 possible variants that obey the K-S relationship, and the misorientations between given pairs of the variants are very specific (Table I). The total fraction of the intervariant boundaries was measured to be around 59 pct of the total grain-boundary area, thus confirming the transformation character of the misorientation distribution.

For the analysis of the variant selection occurring during martensitic transformation, the intervariant misorientations are often represented as those between V1 and other variants, as shown in Table II. To examine the possibility of the variant selection to occur in the studied material, the area fractions of variant boundaries were determined, as shown in Figure 3(b). (Considering a limited accuracy of the EBSD technique, the boundary fractions were measured within a 5-deg tolerance. This led to overlapping of some intervariant boundaries, *e.g.*, V3 and V5, V9 and V19.) A clear preference for V1/V2, V1/V3 (or V1/V5), and V1/V4 variant boundaries provided evidence for noticeable nonrandom variant selection during the martensitic transformation.

To the best of the authors' knowledge, the variant selection occurring during martensitic transformation of 12Cr steel has never been reported previously. One of the possible explanations for this effect may be crystallographic texture, which perhaps evolves in the high-temperature austenitic phase due to severe deformation imposed during FSW. At present, however, this suggestion is totally speculative and requires experimental validation.

The revealed variant-selection effect provides a useful insight into martensitic transformation occurring in the heat-resistant steels, thereby enriching our fundamental understanding of this phenomenon. From a broad perspective, the variant selection should affect grain size as well as crystallographic texture of the martensitic phase, thus influencing mechanical properties of the friction-stir-welded material. On the other hand, a real practical significance of this effect is not clear.

C. *Reconstruction of Prior-Austenite Grain Structure*

An establishment of the orientation relationship governing the martensitic transformation enabled reconstruction of prior-austenite grain structure in the stir zone. In the present study, the approach developed by Gey and Humbert[25] was employed. This method is based on the idea that the martensite variants inherited from the same parent austenite grain are characterized by very specific misorientations, as discussed in Section III–B. Therefore, the grain boundaries between these variants can be readily discriminated from other boundaries in an EBSD map. The remaining boundaries are believed to separate the martensite variants from the different parent austenite grains; *i.e.*, they represent prior-austenite boundaries. In this way, the contours of the prior-austenite grains may be identified in an EBSD map.

The original EBSD grain-boundary map is shown in Figure 4(a). In this map, the low- and high-angle boundaries in the martensitic phase are depicted as red and black lines, respectively. The relatively complex hierarchical microstructure is seen, as mentioned in Section III–A. The reconstruction of the prior-austenite grain structure assuming the K-S orientation relationship is shown in Figure 4(b). Despite the prior-austenite grain boundaries becoming visible, the reconstructed structure was still not very clear. This effect was suggested to be attributable to the relatively large orientation spread within martensite laths, which resulted in overlapping of the martensite variants expected from the K-S and N-W relationships, as shown in Figure 2 and discussed in Section III–A.

Table I. Predicted Misorientations Between Martensitic Variants Expected from the Ideal K-S Orientation Relationship[24]

10.53 deg [0.577; 0.577; 0.577]	20.61 deg [0.955; 0.296; 0]	49.47 deg [0.577; 0.577; 0.577]	57.21 deg [0.714; 0.603; 0.357]
10.53 deg [0.707; 0.707; 0]	21.06 deg [0.912; 0.410; 0]	50.51 deg [0.739; 0.490; 0.462]	57.21 deg [0.738; 0.628; 0.246]
14.88 deg [0.933; 0.354; 0.650]	47.11 deg [0.719; 0.626; 0.302]	50.51 deg [0.767; 0.615; 0.186]	60.00 deg [0.577; 0.577; 0.577]
20.61 deg [0.659; 0.659; 0.363]	49.47 deg [0.707; 0.707; 0]	51.73 deg [0.659; 0.659; 0.363]	60.00 deg [0.707; 0.707; 0]

Table II. Misorientations Between V1 and Other Variants Expected from the Ideal K-S Orientation Relationship[21]

V2	60.0 deg [0.58; − 0.58; 0.58]	V10	50.5 deg [− 0.49; − 0.46; 0.74]	V18	47.1 deg [− 0.30; − 0.63; − 0.72]
V3	60.0 deg [0.00; − 0.71; − 0.71]	V11	14.9 deg [0.35; − 0.93; − 0.07]	V19	50.5 deg [− 0.62; 0.17; − 0.77]
V4	10.5 deg [0.00;0.71;0.71]	V12	57.2 deg [0.36; − 0.71; 0.60]	V20	57.2 deg [− 0.36; − 0.60; − 0.71]
V5	60.0 deg [0.00;0.71;0.71]	V13	14.9 deg [0.93; 0.35;0.07]	V21	20.6 deg [0.96; 0.00; − 0.30]
V6	49.5 deg [0.00; − 0.71; − 0.71]	V14	50.5 deg [− 0.74; 0.46; − 0.49]	V22	47.1 deg [− 0.71; 0.30; − 0.63]
V7	49.5 deg [− 0.58; − 0.58; 0.58]	V15	57.2 deg [− 0.25; − 0.63; − 0.74]	V23	57.2 deg [− 0.73; − 0.25; 0.63]
V8	10.5 deg [0.58; − 0.58; 0.58]	V16	20.6 deg [0.66; 0.66; 0.36]	V24	21.1 deg [0.91; 0.41; 0.00]
V9	50.5 deg [− 0.19; 0.77; 0.62]	V17	51.7 deg [− 0.66; 0.36; − 0.66]		

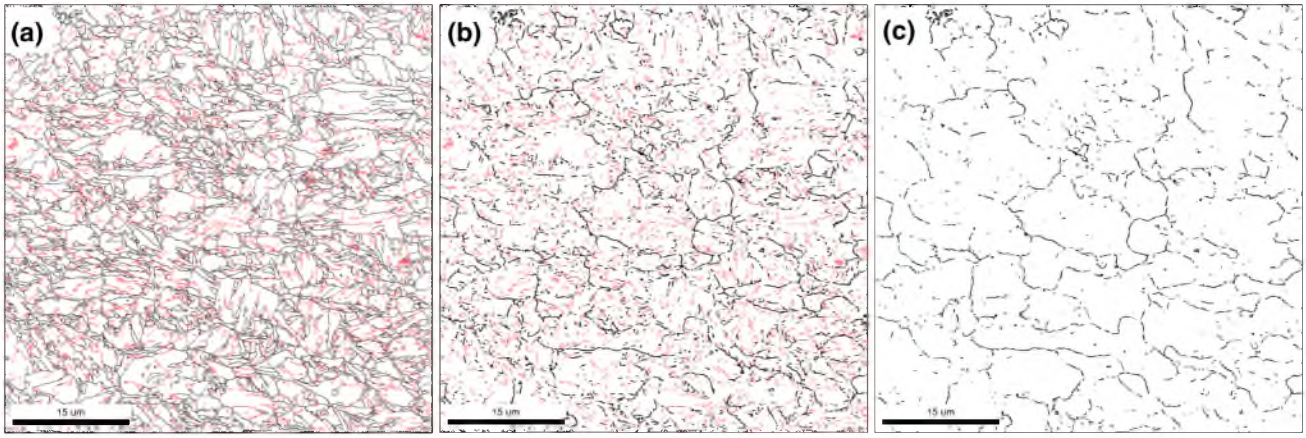

Fig. 4— (*a*) EBSD gram-boundary map of martensitic phase and reconstruction of prior-austenite grain structure assuming the (*b*) K-S orientation relationship or (*c*) mixed orientation relationship. Details are presented in this section.

Table III. Predicted Misorientations Between Martensitic Variants Expected from the Mixed K-S and N-W Orientation Relationships[24]

5.26 deg [0.577; 0.577; 0.577]	20.16 deg [0.814; 0.551; 0.186]	50.87 deg [0.702; 0.579; 0.414]	54.74 deg [0.577; 0.577; 0.577]
5.26 deg [0.707; 0.707; 0]	20.16 deg [0.965; 0.214; 0.151]	50.87 deg [0.716; 0.640; 0.277]	55.66 deg [0.726; 0.492; 480]
11.77 deg [0.907; 0.358; 0.224]	48.57 deg [0.702; 0.669; 0.244]	52.14 deg [0.716; 0.613; 0.332]	57.84 deg [0.695; 0.672; 0.256]
11.77 deg [0.848; 0.483; 0.218]	48.57 deg [0.733; 0.559; 0.387]	52.14 deg [0.730; 0.627; 0.272]	58.83 deg [0.692; 0.691; 0.205]
17.19 deg [0.977; 0.154; 0.149]	49.73 deg [0.663; 0.537; 0.522]	54.74 deg [0.707; 0.707; 0]	58.83 deg [0.717; 0.549; 0.429]
17.19 deg [0.799; 0.548; 0.246]	49.73 deg [0.741; 0.664; 0.946]	54.74 deg [0.577; 0.577; 0.577]	60.21 deg [0.650; 0.538; 0.538]

To account for this effect, the prior-austenite grain structure was reconstructed using the mixed orientation relationship, *viz*. $\{111\}\gamma \parallel \{110\}_{\alpha'}$, $\langle 110\rangle\gamma \parallel \langle 111\rangle_{\alpha'}$, and $\langle 112\rangle\gamma \parallel \langle 110\rangle_{\alpha'}$. The intervariant misorientations expected for this relationship are summarized in Table III. The reconstruction revealed a notably clearer picture of the prior-austenite grain structure (Figure 4(c)), perhaps indicating a reliability of the suggested approach.

As follows from the reconstructed EBSD map, the prior-austenite structure was relatively fine grained with the mean grain size of ~ 15 μm. Considering the large deformation imposed during FSW, as well as the high-temperature character of this process, the observed effect may originate from recrystallization presumably occurring in the high-temperature austenitic phase. On the other hand, the available microstructural data are not enough for a convincing conclusion to be drawn; therefore, this issue warrants further study.

D. *Microstructural Aspects of FSW*

Considering FSW as a potent candidate for the joining of 12Cr steel, it is useful to compare the FSW-induced microstructure with those produced by conventional fusion techniques. Due to material melting as well as the relatively low cooling rate inherent to the fusion-based approaches, the final weld structure is usually characterized by relatively coarse (often columnar) grains and a very high fraction of ferritic phase.[7 12] This normally leads to degradation of material strength and thus necessitates a postweld heat treatment. In contrast, FSW results in a relatively fine-grained microstructure (Figures 1(a) and 4), which is dominated by the martensitic phase.[14] This effect is obviously attributable to the relatively low welding temperature and short thermal exposure as well as to the relatively high cooling rate associated with the FSW process. Moreover, development of the fine-grained microstructure during FSW is also attributed to the relatively large strains experienced by the welded material. The strain-based character of FSW is probably also responsible for the prominent variant selection occurring during martensitic transformation as well as for a relatively large orientation spread within the martensite.

IV. CONCLUSIONS

In this work, EBSD was applied to investigate the martensite crystallography in friction-stir-welded 12Cr heat-resistant steel. Local orientation measurements demonstrated that the martensitic transformation was governed by the K-S orientation relationship and was characterized by large orientation spread within the martensite crystals. The latter effect was attributed to the dilatation effect associated with the martensitic transformations. The analysis of misorientation distribution revealed clear crystallographic preference for the V1/V2, V2/V3, and V1/V4 intervariant boundaries, evidence of nonrandom variant selection occurring during the transformation.

Due to the specific nature of the FSW process involving very large strains, the characteristics of the resulting martensitic phase were deduced to include a relatively fine-grained microstructure, limited number of crystallographic variants, and essential orientation spread.

ACKNOWLEDGMENTS

This work was supported by the Global COE Program in Materials Integration International Center of Education and Research at Tohoku University and partially by the Anhui Provincial Natural Science Foundation (Grant No. 1808085ME150).

REFERENCES

1. F. Abe, T.U. Kern, and R. Viswanathan: *Creep-Resistant Steels*, Woodhead Publishing Limited, Cambridge, United Kingdom, 2008, pp. 26–42.
2. K. Maruyama, K. Sawada, and J. Koike: *ISIJ Int.*, 2001, vol. 41, pp. 641–53.
3. F. Abe: *J. Press. Vessel Technol.*, 2016, vol. 138, p. 040804.
4. J.P. Fernandes, E.M.D. Lopes, and V. Maneta: *J. Eng. Gas Turb. Power*, 2010, vol. 132, p. 051801.
5. F. Abe: *Development of Creep-Resistant Steels and Alloys for Use in Power Plants*, Woodhead Publishing Limited, Cambridge, United Kingdom, 2014, pp. 250–93.
6. H. Cerjak, P. Hofer, and B. Schaffernak: *ISIJ Int.*, 1999, vol. 39, pp. 874–88.
7. J. Onoro: *Int. J. Pres. Ves. Pip.*, 2006, vol. 83, pp. 540–45.
8. J. Onoro: *J. Mater. Proc. Technol.*, 2006, vol. 180, pp. 137–42.
9. B. Rivolta, F. Tavasci, R. Gerosa, and J. Yenus: *Mater. Perform. Charact.*, 2017, vol. 6, pp. 160–73.
10. E. Taban, A. Dhooge, and E. Kaluc: *Mater. Manufac. Proc.*, 2009, vol. 24, pp. 649–56.
11. K. Fujiyama, K. Mori, T. Matsugana, H. Kimachi, T. Saito, T. Hino, and R. Ichii: *Mater. Sci. Eng. A*, 2009, vols. 510–511, pp. 195–201.
12. R.M. Hunt, B. El-Dasher, B.W. Choi, and S.G. Torres: *Fus. Eng. Des.*, 2014, vol. 89, pp. 1617–22.
13. W.M. Thomas, C.S. Wiesner, D.J. Marks, and D.G. Staines: *Sci. Technol. Weld. Join.*, 2009, vol. 14, pp. 247–53.
14. P. Hua, S. Mironov, C.Z. Nie, Y.S. Sato, H. Kokawa, S.H.C. Park, and S. Hirano: *Sci. Technol. Weld. Join.*, 2014, vol. 19, pp. 76–81.
15. Y.S. Sato, H. Kokawa, H.T. Fujii, Y. Yano, and Y. Sekio: *Metall. Mater. Trans. A*, 2015, vol. 46A, pp. 5789–5800.
16. Y. Yano, Y.S. Sato, Y. Sekio, S. Ohtsuka, T. Kaito, R. Ogawa, and H. Kokawa: *J. Nucl. Mater.*, 2013, vol. 442, pp. S524–28.
17. F.C. Liu, Y. Hovanski, M.P. Miles, C.D. Sorensen, and T.W. Nelson: *J. Mater. Sci. Technol.*, 2018, vol. 34, pp. 39–57.
18. C. Zhang, L. Cui, D. Wang, Y. Liu, and H. Li: *Mater. Sci. Eng. A*, 2018, vol. 729, pp. 257–67.
19. Y.H. Guo, Y.Q. Chang, J. Zhang, J.Z. Lic, S. Ukai, and F.R. Wan: *Sci. Technol. Weld. Join.*, 2018, vol. 23, pp. 50–57.
20. H. Dawson, M. Serrano, R. Hernandez, S. Cater, and E. Jimenez-Melero: *Mater. Sci. Eng. A*, 2017, vol. 693, pp. 84–92.
21. A. Stormvinter, G. Miyamoto, T. Furuhara, P. Hedstrom, and A. Borgenstam: *Acta Mater.*, 2012, vol. 60, pp. 7265–74.
22. H. Kitahara, R. Ueji, N. Tsuji, and Y. Minamoto: *Acta Mater.*, 2006, vol. 54, pp. 1279–88.
23. H. Kitahara, R. Ueji, M. Ueda, N. Tsuji, and Y. Minamoto: *Mater. Character.*, 2005, vol. 54, pp. 378–86.
24. B. Sonderegger, S. Mitsche, and H. Cerjak: *Mater. Charact.*, 2007, vol. 58, pp. 874–82.
25. N. Gey and M. Humbert: *Acta Mater.*, 2002, vol. 50, pp. 277–87.